International Symposium
On Turbulence and Shear Flow
Phenomena (TSFP-9)
June 30 - July 3, 2015 *Melbourne, Australia*

INVESTIGATION OF A TURBULENT FLOW FROM THE TRANSITIONALLY ROUGH REGIME TO THE FULLY ROUGH REGIME

L. Chan, M. MacDonald, N. Hutchins, D. Chung & A. Ooi
Department of Mechanical Engineering
University of Melbourne
Victoria 3010, Australia
lzhchan@unimelb.edu.au

ABSTRACT

Direct Numerical Simulations (DNS) are carried out in a turbulent rough-wall pipe at low and medium Reynolds numbers. The rough surface, which is comprised of three-dimensional sinusoidal roughness elements, was viscously scaled from the transitionally rough regime to the fully rough regime. The main aim of this study is to analyse the behaviour of the near-wall cycle as the surface condition changes from smooth through to fully rough. When analysing the streamwise velocity, a triple decomposition is used to distinguish between the fluctuations due to the spatial variation with the actual turbulent fluctuations. For small roughness height ($h^+ < 15$), the near-wall cycle streaks occurs above the roughness elements. Although the high and low speed streaks look similar to the smooth wall when visually inspected, subtle differences are observed when the premultiplied energy spectra are analysed. When the flow is fully rough, the near-wall cycle is replaced by the stationary features of the flow which dominate within the roughness elements. We also analyse the contribution of the apparent wall shear stress due to form (pressure) drag (τ_R) expressed as a ratio between form and total shear stress ($R_\tau = \frac{\tau_R}{\tau_T}$). In the fully rough regime, the form drag dominates ($R_\tau > 0.75$) and disrupts the near-wall cycle. Townsend's outer layer similarity is observed when the wall normal height normalised by the mean radius of the pipe y/R_0 is greater than 0.56, where a collapse in the streamwise premultiplied energy spectra is obtained.

INTRODUCTION

Rough wall-bounded turbulent flow has been extensively investigated due to its many practical applications. Being able to predict the drag caused by a given rough surface (e.g: the surface of a ship's hull or aircraft fuselage) is critical to estimating the propulsive requirements for many engineering system. A better understanding of the physics of roughness-affected turbulent flow will enable researchers to develop more accurate drag prediction models.

With the advancement of computing power, Computational Fluid Dynamics (CFD) is becoming an important tool in understanding rough-wall bounded turbulent flows. CFD is able to provide complete three-dimensional information of the flow field which is very difficult to obtain experimentally. In this paper, a turbulent flow through a rough-wall pipe is simulated from the transitionally rough to the fully rough regime. The roughness elements of the pipe consist of three dimensional sinusoidal roughness. Current work is inspired by Shockling *et al.* (2006) and Schultz & Flack (2007) who carried out experiments on a honed rough pipe and on a rough boundary layer (where the roughness was geometrically similar to the honed pipe) respectively. In these studies, the flow varies from the hydraulically smooth to the fully rough regime by changing the Reynolds number of the flow, which effectively increases the roughness Reynolds number $k_s^+ = k_s U_\tau/\nu$ while maintaining the physical size of the roughness. For the roughness cases simulated in this paper, the roughness elements will be geometrically scaled and simulated at $Re_\tau = 180$ and 540.

NUMERICAL METHOD

The turbulent flow through a pipe is solved using the Navier–Stokes equations for incompressible flow in Cartesian coordinates:

$$\nabla \cdot \mathbf{u} = 0, \tag{1a}$$

$$\frac{\partial \mathbf{u}}{\partial t} + \mathbf{u}\cdot\nabla\mathbf{u} = -\frac{1}{\rho}\nabla p + \nu\nabla^2\mathbf{u} + F_x\mathbf{i}, \tag{1b}$$

where $\mathbf{u} = (u, v, w)$ is the velocity in the x, y, and z directions, t is time and $F_x(t)$ is the uniform, time-varying body force required to maintain a constant mass flux through the pipe. A finite-volume unstructured collocated code is used to solve the Navier–Stokes equations (for further details refer to Chan *et al.* (2015)). A Cartesian 'O-grid' mesh is used for the simulations instead of a cylindrical polar mesh as it allows for better control of the number of grid points in the azimuthal direction, which is fixed for a cylindrical polar mesh at all wall normal distances. The no-slip condition is applied to the walls of the pipe and a periodic boundary condition is applied in the streamwise direction. The length of the pipe is selected to be $L_x = 4\pi R_0$ where R_0 is the reference radius which we have set to be equal to the mean radius of the pipe $\overline{R}$. For all of the simulated cases, the viscous wall-normal spacing of the first grid cell from the wall is less than 0.3 (i.e. $\Delta y^+ < 0.3$) to ensure the near wall flow is fully resolved. The grid is largest at the centre of the pipe where it is approximately cube shaped ($\Delta r\theta^+ \approx \Delta r^+ \approx \Delta x^+$). The largest grid spacing is limited to less than 6.5 viscous units to ensure that all turbulent scales

are fully resolved. Table 1 summarises the mesh parameters of the cases simulated.

Table 1. Computational details of the meshes used for $Re_\tau = 180$ and 540 simulations and its associated symbols. $N_{r,\theta}$ is the number of elements in an (r,θ) plane, N_x the number of elements in the streamwise direction and N_{λ_x} the number of elements per roughness wavelength. Δr^+ and $\Delta z^+ \approx \Delta r\theta^+$ are the mean grid spacings in wall-units at the wall calculated using the local instantaneous u_τ. The largest cells are located at the centre of the pipe where $\Delta r^+ \approx \Delta r\theta^+ \approx \Delta x^+$.

Case	Sym	$N_{r,\theta}$	N_x	N_{λ_x}	Δr^+	Δx^+
	$Re_\tau = 180$					
Smooth	○	13685	384	-	0.33	6.1
02_018	●	24864	512	4	0.12	3.5
05_035	●	24864	512	8	0.12	3.4
10_070	●	24864	512	16	0.11	3.2
13_094	●	24864	512	21	0.11	3.3
16_113	●	24864	512	26	0.16	3.2
20_141	●	19872	512	32	0.11	3.2
	$Re_\tau = 540$					
Smooth	○	94752	1152	-	0.23	5.8
20_141	●	104400	1152	24	0.14	4.4
40_283	●	104400	1152	48	0.13	4.1
60_424	●	108720	1152	72	0.15	4.0
80_565	●	108720	1152	96	0.14	3.8

SURFACE ROUGHNESS

The rough surface of the pipe, R, is described by a cosine function as given by,

$$R(x,\theta) = R_0 + h\cos\left(\frac{2\pi x}{\lambda_x}\right)\cos\left(\frac{2\pi R_0\theta}{\lambda_s}\right) \qquad (2)$$

where the reference radius of the pipe R_0, is set to be the mean radius of the pipe $\overline{R}$ (which is also the virtual origin of the pipe), h is the semi-amplitude of the sinusoidal roughness (half of the peak-to-trough height $k_t = 2h$) and λ_x and λ_s are the wavelengths of the roughness elements in the streamwise and azimuthal directions respectively. For all of the rough cases, $\lambda_x = \lambda_s$ and the surface has a roughness semi-amplitude to wavelength ratio of $h/\lambda_x = 0.141$. All the roughness elements have a root-mean-square roughness height that is twice the roughness semi-amplitude $k^+_{rms} = 2h^+$ and an effective slope ES of 0.361 (defined by Napoli *et al.* (2008) as the mean of the absolute streamwise gradient). ES is twice the solidity Λ. However, for case 02_018 and 05_035, due to the insufficient number of grid points per roughness element, the surface is faceted and therefore the true value of ES is underestimated (10% less for case 02_018). Throughout the paper, the roughness cases are identified by the following identifying code

$$\underbrace{\boxed{1}\boxed{0}}_{h^+} - \underbrace{\boxed{1}\boxed{4}\boxed{1}}_{\lambda^+} \qquad (3)$$

where the first two digits represent the roughness semi-amplitude and the last three digits represent the streamwise or spanwise wavelength of the roughness elements (both in viscous units). In this paper, the roughness elements are geometrically scaled (fixed h/λ ratio) for roughness semi-amplitude values of $h^+ = 2.5, 5, 10, 13.3, 16$ and 20 at $Re_\tau = 180$ and for $h^+ = 20, 40, 60$ and 80 at $Re_\tau = 540$.

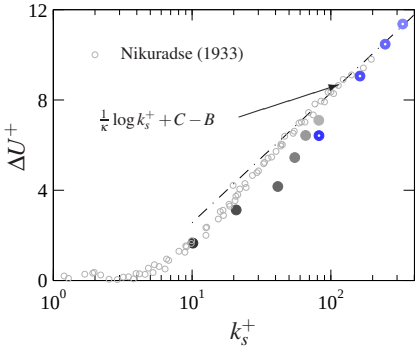

Figure 1. Plot of roughness function ΔU^+ against equivalent sandgrain roughness height k_s^+. Symbols are as in table 1.

ROUGHNESS FUNCTION

The roughness elements cause a downward shift in the mean streamwise velocity profile when scaled in viscous units. This shift is measured by the roughness function ΔU^+ in the modified logarithmic law (Hama, 1954),

$$U^+ = \frac{1}{\kappa}\ln(y^+) + C - \Delta U^+ \qquad (4)$$

where $\kappa = 0.4$ and $C = 5.3$ for current simulations. ΔU^+ is measured 50 wall-units above the crest of the roughness elements as the log region of the flow at low and moderate Reynolds numbers is poorly defined. The roughness function is plotted in figure 1 against the equivalent sand grain roughness k_s^+ of Nikuradse (1933). The flow, which is initially in the transitionally rough regime, approaches the fully rough regime as the size of the viscously scaled roughness elements increases. For $h^+ > 60$, the flow is in the fully rough regime since the variation of ΔU^+ with k_s^+ falls on to the fully rough asymptote. Note that if we assume Nikuradse's constant $B = 8.5$ (Nikuradse, 1933), this suggests that $k_s^+ = 4.1h^+$. The three-dimensional sinusoidal roughness reaches the fully rough asymptote when $k_s^+ \approx 200$– a value far greater than the one obtained by Nikuradse's sand grain roughness ($k_s^+ \approx 40$). There is a slight difference in ΔU^+ for case 20_141 when simulated at $Re_\tau = 180$ and 540 and this is due to the low Reynolds number effect of the smooth wall pipe at $Re_\tau = 180$ (Chan *et al.*, 2015).

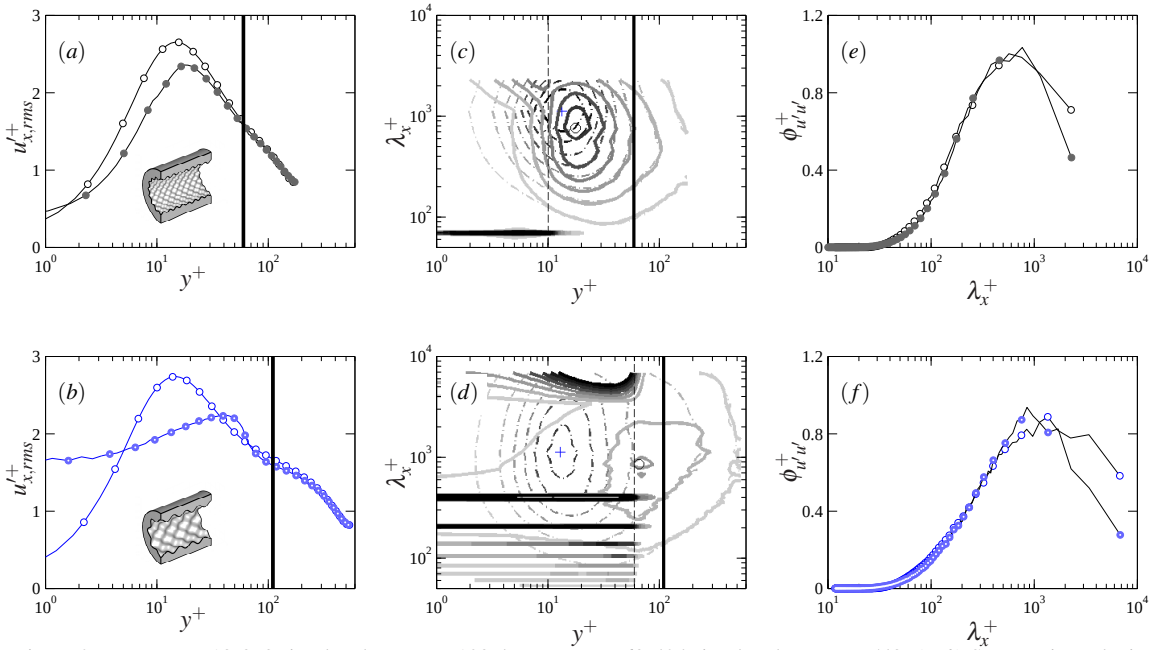

Figure 2. Top: case 10_070 simulated at $Re_\tau = 180$, bottom: case 60_424 simulated at $Re_\tau = 540$. (a, b) Streamwise velocity fluctuations $u'_{x,rms}$ (sketch of the roughness inset of the plot), (c, d) contour of streamwise premultiplied energy spectra $\phi^{+}_{u'u'}$. Symbols $+$ and $\circ$ shows the location of the near wall peak for the smooth wall and rough wall respectively. Solid black lines in (a, b, c, d) are located 50 wall-units above the crest of the roughness and corresponds to the location of the (e, f) streamwise premultiplied energy spectra (at $y^+ = 60$ and $y^+ = 110$ respectively). Symbols are as in table 1.

NEAR WALL STRUCTURE

In this section, case 10_070, which is in the transitionally rough regime and case 60_424, which is in the fully rough regime, will be analysed with greater detail and compared with the turbulent smooth wall flow. The streamwise velocity fluctuation ($u'^{+}_{x,rms}$) profiles are illustrated in figure $2(a, b)$. For the smooth wall case, the maximum streamwise velocity fluctuation is located at $y^+ \approx 15$ and this peak is associated with the near-wall cycle where organised structures are observed (Kline *et al.*, 1967; Jimenez *et al.*, 2004). The appearance of roughness causes the maximum $u'^{+}_{x,rms}$ to decrease. This phenomena, is also well recorded in the literature (Grass, 1971; Krogstad *et al.*, 2005). and consistent with current observation. In addition, the location of the maximum $u'^{+}_{x,rms}$ also changes with the roughness height. For cases with $h^+ < 15$, the location of the peak appears to be only slightly affected and occurs above the roughness elements (eg. for case 10_070, maximum $u'^{+}_{x,rms}$ located at $y^+ \approx 18$ as observed in figure $2(a)$). On the other hand, it appears that, for the roughness cases tested, the maximum $u'^{+}_{x,rms}$ is located within the roughness elements when $h^+ > 15$. This is explicitly observed in figure $2(b)$ where for case 60_424, the location of maximum $u'^{+}_{x,rms}$ appears to have been shifted from its usual smooth wall location of $y^+ = 15$ to $y^+ \approx 42$. The solid vertical black lines in figure $2(a, b)$ are located 50 wall units above the roughness element. At this location, Townnsend's outer-layer similarity is observed in the mean velocity profiles of all the rough cases (Chan *et al.*, 2015). This is however not the case for the streamwise velocity fluctuation ($u'_{x,rms}$) profile of the fully rough case 60_424 where the velocity fluctuations are slightly underestimated compared to the smooth wall.

Next, the premultiplied energy spectra of the flow is investigated to identify the dominant turbulent scales in the flow. To calculate the premultiplied energy spectra of the flow, the Cartesian grid is first interpolated to a cylindrical polar grid using a third order cubic polynomial. To minimise the interpolation error, the cylindrical polar grid are mapped as close as possible to the Cartesian grid. The contours of the streamwise premultipled spectra of the streamwise velocity ($\phi^{+}_{u'u'}$) of the rough walls (solid lines) are plotted in figure $2(c, d)$ with the contours of the smooth wall at the same friction Reynolds number overlaid in the background (dash-dotted lines) for comparison. The contours of the smooth wall are not fully closed, indicating that the length of the pipe used insufficiently long to decorrelate the largest structures in the flow. However, the pipe length independence study conducted by Chin *et al.* (2010) found that the turbulence intensity of the flow is fully converged for the domain length used here. In addition, as the length of the pipe is the same for both the smooth and rough cases, any differences emerging from the premultiplied spectra would be due to the roughness. Analysing the streamwise premultiplied energy spectra at $y^+ = 60$ for case 10_070 in figure $2(e)$, a reduction in the energy in the largest scales is observed despite the streamwise velocity fluctuation ($u'_{x,rms}$) at that location being almost the same as the smooth wall. A reduction in energy in the largest scales is also observed in case 60_424 at $y^+ = 110$ (see figure $2(f)$) and it appears that energy is slightly redistribution and is concentrated at $\lambda_x^+ \approx 850$ which is about twice the wavelength of the roughness. Only far away from the roughness elements when $y^+ > 100$ for case 10_070 and when $y^+ > 300$ for case 60_424, do the contours of the rough wall coincide with the contours of the smooth wall. Therefore, Townsend's outer layer hypothesis only appears to be satisfied when $y/R_0 > 0.56$ when considering the pre-

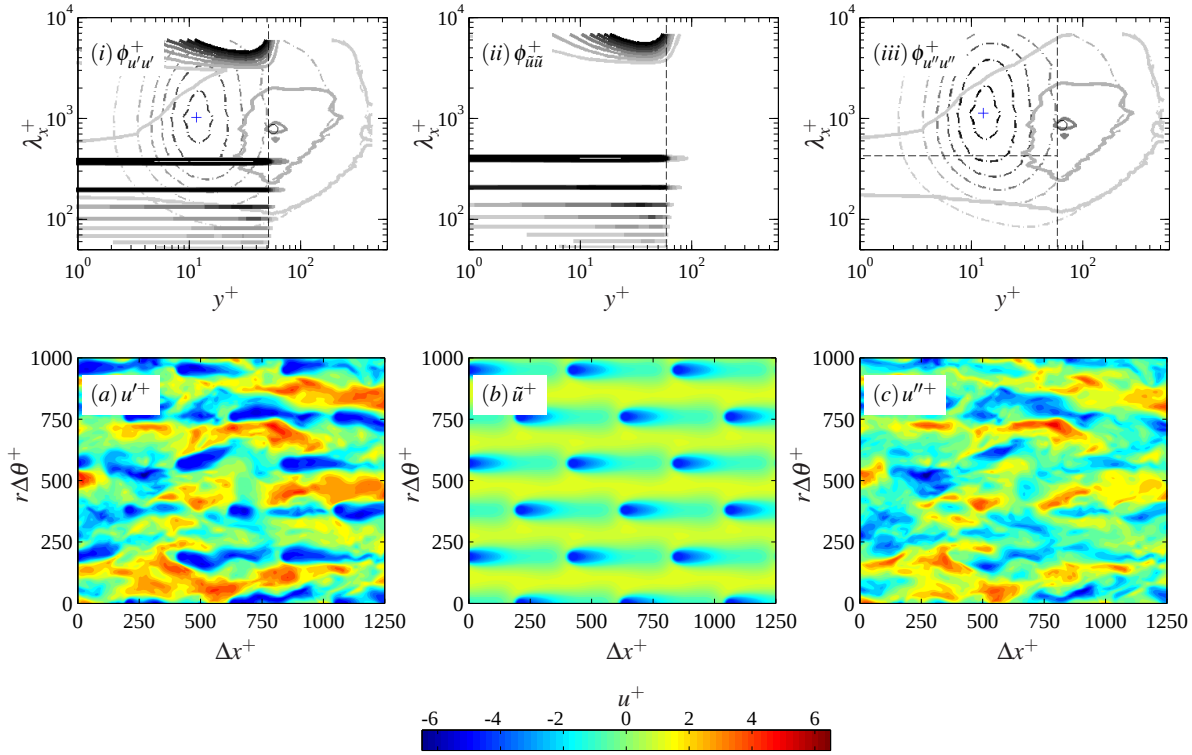

Figure 3. Contour of the streamwise premultiplied spectra of the streamwise velocity fluctuation about the (i) global mean (u'^+) and (ii) time-averaged mean (u''^+). Dashed horizontal and vertical lines corresponds to the wavelength and height of the roughness elements respectively. Contour of the (a) streamwise velocity fluctuations u'^+, (b) time-averaged spatial variation of the streamwise velocity $\tilde{u}^+$ and (c) streamwise velocity turbulent fluctuation u''^+ at the crest of the roughness elements $y^+ = 60$ for case 60_424 simulated at $Re_\tau = 540$.

multiplied spectra. In a smooth turbulent boundary layer, Jimenez *et al.* (2004) found that the occurrence of the organised low and high speed streaks have a streamwise length of $\lambda_x^+ \approx 1000$ which are located at $y^+ \approx 15$ (as observed in current smooth wall simulations (dot-dashed contours) in figure 2(c,d)). Now, for a rough wall turbulent boundary layer, there is some suggestion in the literature that transitionally rough surfaces weaken the 'viscous generation cycle' (Jimenez, 2004). It can be seen in figure 2(c) that the peak of the streamwise premultiplied energy spectra for case 10_070 is weaker compared to the smooth wall and the streamwise wavelength is shortened to $\lambda_x^+ \approx 853$. This is due to the roughness elements breaking up the long and streaky structures which normally exist in a smooth wall turbulent flow. For the fully rough case 60_424, the near wall cycle of the smooth wall resides within the roughness elements. Within the roughness elements, the energy spectra is calculated by zero padding the area occupied by the roughness elements. While this physically models the flow, the zero padding reduces the actual $u'^+_{x,rms}$ when calculated from the spectra. This difference becomes more prominent further within the roughness and therefore one has to be careful when interpreting the premultiplied energy spectra in this region. It can be seen in figure 2(c,d) that the contours of the streamwise premultipled spectra of the streamwise velocity $(\phi^+_{u'u'})$ of the rough wall (solid contour lines) is different to the smooth wall (dash-dotted contour lines) at regions near the roughness. It can be seen in figure 2(c,d) that within the roughness elements, there are structures that are infinitely long and high energy structures at discrete wavelengths. These structures are due to the contribution of the spatial variation of the rough surface. Therefore, in a rough wall, the streamwise velocity component can be decomposed into three components (Coceal & Belcher, 2004),

$$u = U + \tilde{u} + u'' \tag{5}$$

where $U = <\overline{u}>$ is the spatial and temporal averaged mean, which is also known as the global mean and $\tilde{u} = \overline{u} - U$ is the spatial variation of the time-averaged flow around individual roughness, elements and $u'' = u - \overline{u}$ is the fluctuation about the time averaged mean, known as the turbulent fluctuation. u'' is not to be confused with u' which is the fluctuation about the global mean which contains both the turbulent fluctuation and fluctuations due to the spatial variation. For a smooth wall, $\tilde{u} = 0$ and therefore $u' = u''$. This method of decomposition was initially used in analysing plant canopy flows where the rough surfaces are spatially inhomogeneous (Raupach & Shaw, 1982; Finnigan, 1985, 2000)

Using this decomposition, the streamwise premultiplied spectra of the streamwise velocity for case 60_424 is analysed. Contours of the premultiplied energy spectra of u', $\tilde{u}$ and u'' are plotted in figure 3(i,ii,iii) respectively. On the left of figure 3 are the contours of the corresponding velocity fluctuation at the crest of the roughness elements. From visual inspection of figure 3(a), it appears that the low and high speed streaks are confined by the roughness elements. However, there are stationary features in the flow where from figure 3(b) it is observed that the high speed

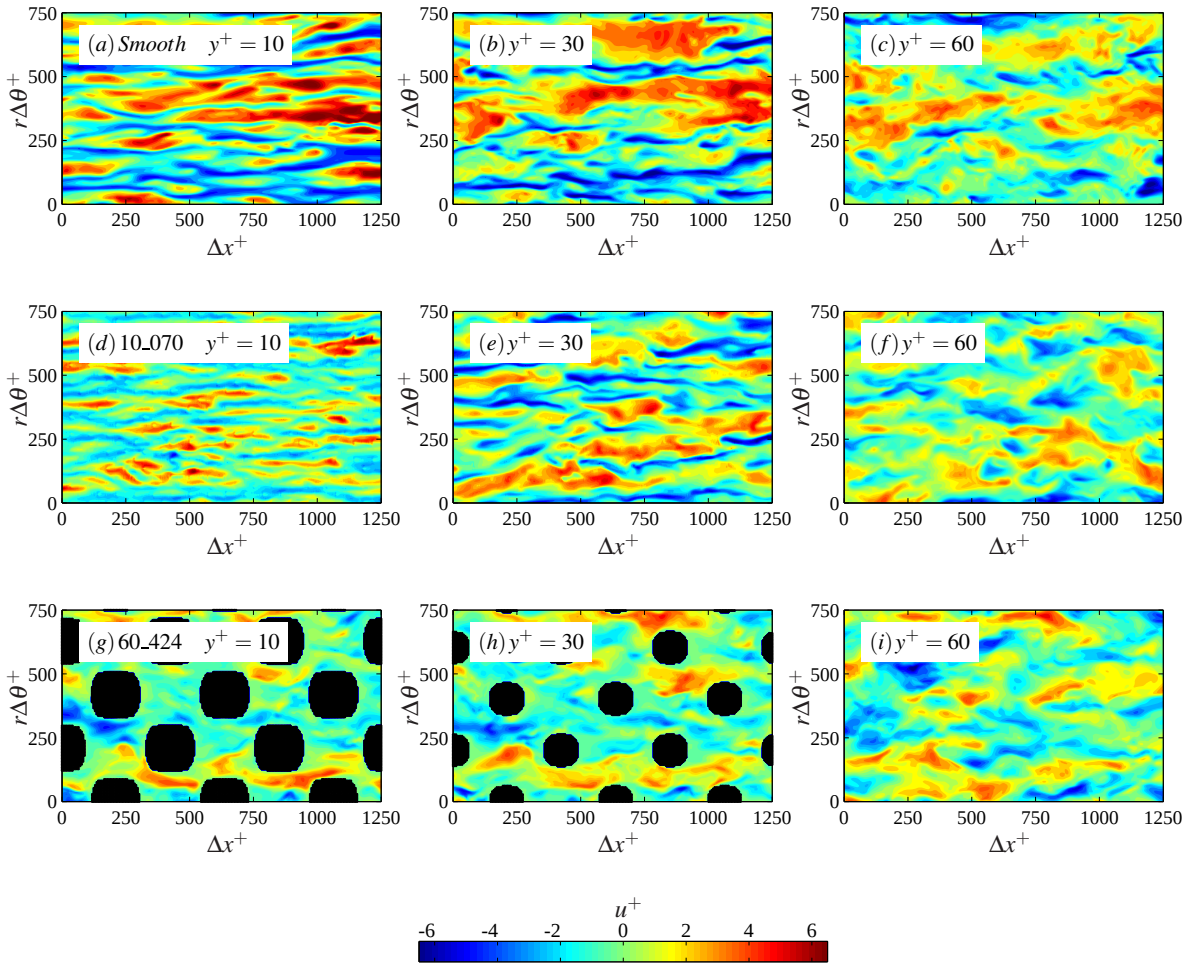

Figure 4. Contour of the streamwise velocity turbulent fluctuation u''^+ of the (top) smooth wall, (middle) case 10_070 and (bottom) case 60_424 at annular location $y^+ = 10, 30$ and 60. Black filled contours indicate the roughness elements.

fluid resides in between the roughness elements, which is the path of least resistance, and this is reflected in the premultiplied energy spectra profile in figure 3(*ii*) as the energy occurring at the largest streamwise wavelength. On the other hand, the discrete energy peaks in the spectra coincide with the wavelength of the sinusoidal roughness elements and its harmonics. These features are unique to the homogenous sinusoidal roughness which we have simulated and would be very different compared to a realistic inhomogenous roughness. Removing the stationary features in the flow, we obtain the velocity fluctuations purely due to turbulence. Within the roughness elements, the turbulent fluctuations are weak and the streamwise wavelength of the structures are centred around the wavelength of the roughness elements. It is interesting to note that the velocity fluctuations due to spatial variation of the roughness $\tilde{u}$ are affected only up to 30 wall units above the roughness (where viscosity dominates) while the turbulent velocity fluctuations u'' are affected to a greater extend (as seen in figures 3(*ii*, *iii*)). In figure 4, we visually compare the instantaneous turbulent fluctuations of the streamwise velocity u''^+ for cases 10_070 and 60_424 with the smooth wall at three different annular locations. At annular location of $y^+ = 10$, which corresponds to the crest of the roughness for case 10_070, is it obvious that the long streaky structures are broken down and are not as intense as the smooth wall at the same wall normal location (see figure 4(*a*, *d*). Further away at $y^+ = 30$, there is an increase in the turbulent fluctuations for case 10_070 and it appears that the structures are much longer than at $y^+ = 10$. Qualitatively, these streaky structures are quite similar to the smooth wall at the same wall normal location (see figure 4(*b*, *e*)), but we know quantitatively that there are subtle differences in the flow when analysing the premultiplied spectra at that wall normal location (refer back to figure 2(*c*)). For case 60_424, the flow resides within the roughness elements at these wall normal locations and the intensity u''^+ is weak compared to the smooth wall. At $y^+ = 60$, the near wall streaks of the smooth wall are not observed in all three cases. However, it is noticeable that the roughness elements of case 60_424 have reduced the length of the high speed fluid structures (compare figure 4(*c*, *i*)).

PRESSURE AND VISCOUS DRAG RATIO

In the fully rough regime, it is often assumed that the pressure drag dominates the viscous drag in the flow. An important parameter used is the ratio of the apparent wall shear stress due to form drag on the roughness elements to the total wall shear stress $R_\tau = \tau_R/\tau_T$. Scaggs *et al.* (1988)

who conducted rough pipe experiments on hemispheres and cones found R_τ be to at least 0.8 when the flow is fully rough. For the current sinusoidal roughness simulated, the flow is fully rough when $R_\tau \approx 0.75$ (as observed in figure 5) where the pressure drag is dominant and replaces the near wall cycle of a smooth wall. An interesting observation is that R_τ increases approximately linearly with the log of h^+ even in the transitionally rough regime. However, it is possible for a surface to be fully rough with $R_\tau = 0$. Atypical roughnesses such as straight riblets, which reduces drag when transitionally rough, contains no streamwise pressure drag component when the flow is fully rough. Work by Garca-Mayoral & Jimnez (2011) found two-dimensional Kelvin-Helmholtz-like instability in the streamwise velocity which may have caused the drag increase.

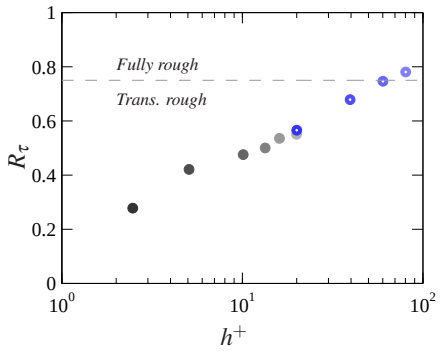

Figure 5. Plot of the ratio of the apparent wall shear stress due to form drag on the roughness elements to the total wall shear stress R_τ against roughness height h^+.

CONCLUSIONS

DNS is carried out at $Re_\tau = 180$ and 540 over a three-dimensional sinusoidal roughness where the flow ranged from the transitionally rough regime to the fully rough regime. For case 10_070 which is in the transitionally rough regime, the near wall streaky structure seems to persist despite the presence of the roughness elements. However, as the viscous size of the roughness increases, the pressure drag component of the flow becomes more dominant and weakens the 'viscous generation cycle' which occurs naturally in a smooth wall- bounded turbulent flow. For the simulated three-dimensional sinusoidal roughness elements, we estimate that the surface is in the fully rough regime when pressure drag accounts for approximately 75% of the total drag. In addition, the near wall peak of the streamwise premultiplied energy spectra is completely replaced by the stationary features of the roughness elements when the flow is fully rough. Townsend's outer layer similarity is satisfied when $y/R_0 > 0.56$ where there is a collapse in the premultiplied spectra of the streamwise velocity between the smooth and rough case. This collapse is much further than the collapse observed when considering the mean velocity profile as described by Chan *et al.* (2015).

ACKNOWLEDGEMENTS

The authors gratefully acknowledge the financial support of the Australian Research Council (ARC) and the computational time granted under the Resource Allocation Scheme by the Victorian Life Science Computational Institute (VLSCI).

REFERENCES

Chan, L., MacDonald, M., Chung, D., Hutchins, N. & Ooi, A. 2015 A systematic investigation of roughness height and wavelength in turbulent pipe flow in the transitionally rough regime. *J. Fluid Mech.* **771**, 743–777.

Chin, C., Ooi, A. S. H., Marusic, I. & Blackburn, H. M. 2010 The influence of pipe length on turbulence statistics computed from direct numerical simulation data. *Phys. Fluids* **22**, 115107.

Coceal, O. & Belcher, S. E. 2004 A canopy model of mean winds through urban areas. *Quart. J. Roy. Meteorol. Soc.* **130**, 1349–1372.

Finnigan, J. J. 1985 Turbulent transport in flexible plant canopies. In *The Forest-Atmosphere Interaction*, pp. 443–480. Springer.

Finnigan, J. J. 2000 Turbulence in plant canopies. *Annu. Rev. of Fluid Mech.* **32**, 519–571.

Garca-Mayoral, Ricardo & Jimnez, Javier 2011 Hydrodynamic stability and breakdown of the viscous regime over riblets. *J. Fluid Mech.* **678**, 317–347.

Grass, A. J. 1971 Structural features of turbulent flow over smooth and rough boundaries. *J. Fluid Mech.* **50**, 233–255.

Hama, F. R. 1954 Boundary-layer characteristics for smooth and rough surfaces. *Trans. Soc. Naval Archit. Mar. Eng.* **62**, 333–358.

Jimenez, J. 2004 Turbulent flows over rough walls. *Annu. Rev. Fluid Mech.* **36**, 173–196.

Jimenez, J., del Alamo, J. C. & Flores, O. 2004 The large-scale dynamics of near-wall turbulence. *J. Fluid Mech.* **505**, 179–199.

Kline, S. J., Reynolds, W. C., Schraub, F. A. & Runstadler, P. W. 1967 The structure of turbulent boundary layers. *J. Fluid Mech.* **30**, 741–773.

Krogstad, P. A., Anderson, H. I., Bakken, O. M. & Ashrafian, A. 2005 An experimental and numerical study of channel flow with rough walls. *J. Fluid Mech.* **530**, 327–352.

Napoli, E., Armenio, V. & Marchis, M. De 2008 The effect of the slope of irregularly distributed roughness elements on turbulent wall-bounded flows. *J. Fluid Mech.* **613**.

Nikuradse, J. 1933 *Laws of flow in rough pipes*. National Advisory Committee for Aeronautics Washington.

Raupach, M. R. & Shaw, R. H. 1982 Averaging procedures for flow within vegetation canopies. *Bound-Layer Meteor.* **22**, 79–90.

Scaggs, W. F., Taylor, R. P. & Coleman, H. W. 1988 Measurement and prediction of rough wall effects on friction factor–uniform roughness results. *J. Fluids Eng.* **110**, 385–391.

Schultz, M. P. & Flack, K. A. 2007 The rough-wall turbulent boundary layer from the hydraulically smooth to the fully rough regime. *J. Fluid Mech.* **580**, 381.

Shockling, M. A., Allen, J. J. & Smits, A. J. 2006 Roughness effects in turbulent pipe flow. *J. Fluid Mech.* **564**, 267–285.